PHYSICAL REVIEW B, VOLUME 63, 245419

Light isotope separation in carbon nanotubes through quantum molecular sieving

Sivakumar R. Challa,[1] David S. Sholl,[2] and J. Karl Johnson[1,*]
[1]Department of Chemical and Petroleum Engineering, University of Pittsburgh, Pittsburgh, Pennsylvania 15261
[2]Department of Chemical Engineering, Carnegie Mellon University, Pittsburgh, Pennsylvania 15213

(Received 11 January 2001; revised manuscript received 21 March 2001; published 8 June 2001)

The theoretical basis for the phenomenon of quantum sieving is detailed for confined one-dimensional systems. A simple theory is presented to calculate zero-pressure selectivities due to quantum sieving in nanopores. This simple theory is used to evaluate the ability of various carbon nanotubes and interstices of nanotubes to separate mixtures of light-isotope species. Realistic and accurate potentials are used for the interactions between adsorbates and nanotubes. Path integral molecular simulations are also used to determine quantum sieving zero-pressure selectivities. Good agreement is found between the simple theory and detailed path integral calculations. Systems of H_2-T_2, and ^{3}He-^{4}He are studied in this work, as well as CH_4-CD_4 and H_2-HD.

DOI: 10.1103/PhysRevB.63.245419 PACS number(s): 64.75.+g, 05.30.−d, 67.70.+n, 82.60.−s

I. INTRODUCTION

Molecular sieves are microporous materials that can separate components of a mixture based on either size, shape, or differences in chemical affinity. For example, micropores can effect a separation by excluding larger molecules from the pores or selectively adsorbing a molecule based on its polarity. An important property of molecular sieving is that different isotopic species of the same molecule have identical adsorption properties when a classical description of adsorption is used. In contrast to classical molecular sieving, quantum sieving is a phenomenon that preferentially adsorbs heavier isotopes from an isotopic mixture. The separation is not based on size, shape, or chemical affinity, but on differences in the quantum levels of the heavier and lighter molecules confined in the pore. This phenomenon was first predicted theoretically by Beenakker *et al.*[1] for adsorption of hard spheres in a square-well cylindrical tube. High selectivities were predicted from this simple theory for He isotopes at low temperatures and pressures in pores about 4 Å in diameter. We have previously used theoretical and simulation methods to examine quantum sieving in models of micropores that are not restricted to hard-body systems.[2] In our previous work we performed path integral Monte Carlo simulations with accurate potential models to predict that carbon nanotubes can be used to separate isotopic mixtures of molecular hydrogen using quantum sieving. We predicted low-pressure selectivities on the order of 10 000 for T_2 over H_2 adsorbed in nanotubes around 6 Å in diameter at 20 K. Our calculations also indicated that the selectivity would increase with an increase in pressure.

In the present work we expand on previous efforts by examining quantum sieving in nanotubes and interstitial channels for several different isotopic mixtures, including HD-H_2, T_2-H_2, ^{4}He-^{3}He, and CD_4-CH_4. We use a rigorous analytical method to predict the zero-pressure selectivities of these systems and compare results with detailed path integral molecular simulations. Additionally, the effect of temperature, nanotube diameter, and the helicity of the nanotube on quantum sieving is explored.

The separation of hydrogen isotopes by surface adsorption has been observed in several experiments since the 1960s.[3–7] White and co-workers developed theories for isotope separation based on the concept of hindered surface rotation and the difference in total energies of the adsorbed species.[3,4] They estimated separation factors of HD-H_2 and D_2-H_2 adsorbed on alumina at 77.4 K by using a Morse potential for interaction between hydrogen and the adsorbent surface, and found good agreement with experiments. The selectivity values are small, around 2. The parameters in the Morse potential were treated as adjustable parameters in order to give reasonable agreement with experiment results. However, for adsorption over leached glass (SiO_2), the experimental selectivities increased with decreasing temperature much more rapidly than the calculated values. King and Benson present a similar theory for isotope separation and obtain good agreement between their calculations and experimental results of chromatographic separation of hydrogen isotopes over an alumina column at 77.4 K.[5] Maienschein *et al.* used zeolite 13X in an adsorption column to obtain pure DT and T_2 from a mixture of D_2-DT-T_2 at 23.5 K.[6] They compiled isotherms and separation factors for hydrogen isotopes from literature for adsorption on alumina and several zeolite types and predicted adsorption isotherms and selectivities at lower temperatures by extrapolation. More recently, adsorption isotherms of pure H_2, HD, and D_2 in NaA zeolite from 77–120 K have been measured by gravimetric methods.[7] The pore sizes are of nanoscale in these zeolites. However, the pores are not uniform and in some large pores surface adsorption is observed. In agreement with theoretical models of quantum sieving,[1,2] the heavier isotopes adsorb more strongly than the lighter isotopes. The results in Ref. 7 show that the selectivity of D_2 over H_2 in the low-pressure region, that is, the ratio of the single component isotherms, is less than 2 at 77 K.

The experimental and theoretical studies of quantum sieving reviewed above provide at best a partial description of how the effectiveness of quantum sieving depends on the adsorbent's pore size. It is therefore interesting to consider how quantum sieving may occur in a family of microporous materials with variable pore sizes. The main aim of this paper is to examine the selectivities of quantum sieving as a

0163-1829/2001/63(24)/245419(9)/$20.00

function of pore size and temperature for adsorption inside single-walled carbon nanotubes (SWNTs) and in the interstitial channels of SWNT bundles. Carbon nanotubes are made of curved sheets of graphite. They can be synthesized by various methods such as carbon arc vaporization,[8,9] laser ablation,[10] and catalytic decomposition of organic vapors.[11] They are usually produced as closed-end tubes, and either as single-walled carbon nanotubes or multi-walled nanotubes. It is possible to open the caps at the ends of SWNTs through selective oxidation of the caps.[10,12,13] These nanotubes vary in size, from a few angstroms[14,15] to a couple of nanometers in diameter and up to 1 μm in length. The curvature of graphite sheets makes the inside of the tubes energetically more attractive for adsorption than planar graphite. Studies have been done to assess the potential of carbon nanotubes for storing hydrogen and have been reviewed elsewhere.[16–21] Experiments show that nanotubes can indeed adsorb H_2.[22,23] In addition, experiments show the adsorption of other components as well, such as N_2, Xe, and CH_4.[24–26] Single-walled nanotubes form clusters of bundles of tubes in a triangular lattice structure.[10,27] Theoretical calculations show that it is possible to adsorb material inside the interstices in these bundles.[28,29] One experimental study has found ^{4}He adsorbed in interstitial channels of nanotubes, the interstices providing a cylindrical clearance of 2.1-Å diameter.[30] The study does not mention the diameter of the tubes. However, another experimental study based on adsorption of Xe, CH_4, and Ne argues that these gases do not adsorb on interstitial channels.[31] The nanotubes in this study were reported to be 13.8 Å in diameter. The interstices were estimated to be 2.6 Å in diameter, which surprisingly do not show any adsorption despite being larger than the ones employed by Teizer *et al.*[30] A number of simulation studies have investigated classical models of adsorption in nanotubes.[32,33] The strong adsorption capability, high surface area, and narrow pore size distribution make nanotubes promising adsorbents and make them excellent candidates for separation of isotopes by quantum sieving.

In this paper, we focus on adsorption at low pressures. In this limit, intermolecular interactions between adsorbed molecules can be neglected and convenient theories for quantum sieving selectivity are available.[2] It is only reasonable to focus on the low-pressure limit, of course, if the selectivities observed in this limit can be related to those observed under more general conditions. In a forthcoming paper we describe extensive simulations of single and multicomponent adsorption of hydrogen isotopes in SWNTs under nondilute conditions.[34] While these simulations reveal several interesting features, one important conclusion that can be drawn from them is that the selectivity due to quantum sieving at low pressures is an excellent indicator of the selectivities that occur at higher pressures.

II. THEORY

A simple theory for quantum sieving can be derived by considering a binary mixture in equilibrium with an adsorbed phase composed of the same binary components.[1,2] We consider unidimensional pores, although the model could be extended to more complex pore structures. We also consider adsorbates whose potential energy surface (PES) does not exhibit strong corrugation along the pore axis. This appears to be a reasonable description of molecular adsorption in SWNTs, although the topology and PES corrugation of many zeolites is more complex.[2] In the materials we consider here, if the pore diameter is on the order of the size of the adsorbates then the adsorbed phase will be one dimensional. At low densities, motion of adsorbed particles along the axial direction would be unhindered and classical. However, across the pore, adsorbates are strongly localized by the pore wall. As a result, the transverse energy levels become quantized. At low temperatures, adsorbates will reside mostly in their ground states. If E_i is the transverse ground-state energy of component i, the chemical potential of this adsorbed component is given by[20,29]

$$\mu_i^{\mathrm{ads}} = E_i + kT \ln\left(\frac{\rho_i \lambda_i}{q_i}\right), \tag{1}$$

where ρ_i is the number density of component i in the pore, $\lambda_i = \sqrt{2\pi\hbar^2/m_i kT}$ is the de Broglie thermal wavelength, q_i is the internal molecular partition function, m_i is the mass of component i and T is the absolute temperature. Assuming that the bulk phase is an ideal gas at very low pressure, the chemical potential of the same component, μ_i^{bulk}, is

$$\mu_i^{\mathrm{bulk}} = kT \ln\left(\frac{n_i \lambda_i^3}{q_i}\right), \tag{2}$$

where n_i is the bulk phase density of component i. The adsorbed phase is in equilibrium with the bulk phase, so $\mu_i^{\mathrm{ads}} = \mu_i^{\mathrm{bulk}}$. Thus, assuming q_i is the same in the bulk and adsorbed phases,

$$\rho_i = n_i \lambda_i^2 e^{-E_i/kT}. \tag{3}$$

If we now consider the coadsorption of two distinct components, the selectivity of component i over j is defined as

$$S = \frac{x_i/x_j}{y_i/y_j}, \tag{4}$$

where x and y refer to the mole fractions in the adsorbed and bulk phases, respectively. The analysis above yields the selectivity in the limit of low pressure and temperature, which we denote by S_0. Combining Eqs. (3) and (4), we find

$$S_0 = \frac{m_j}{m_i} \exp\left[-\frac{E_i - E_j}{kT}\right]. \tag{5}$$

It is useful to note that S_0 is independent of the bulk phase composition. To appreciate the significance of this expression, it is helpful to consider the simple example of a cylindrical pore where the adsorption potential is a radially symmetric harmonic potential, $V(r) = Kr^2/2$. The ground-state energy of a species of mass m in this two-dimensional potential is $\hbar\sqrt{K/m_i}$. Since two isotopes of the adsorbed species with mass m_1 and m_2 are subject to the same potential, the low-pressure selectivity of component 2 over component 1 is given by

$$S_0=\frac{m_1}{m_2}\exp\left[-\frac{\hbar\sqrt{K}}{kT}\left(\frac{1}{\sqrt{m_2}}-\frac{1}{\sqrt{m_1}}\right)\right]. \tag{6}$$

Thus, if $m_1<m_2$, then $S_0>1$ at low temperatures. That is, the pores selectively adsorb the heavier isotope over the lighter isotope. Although the zero-point energy of isotopes in more realistic PESs does not have the simple form available for the harmonic potential, the qualitative preference for heavy over light isotopes is a generic feature of quantum sieving.

Equation (5) is valid when the quantum confinement of the adsorbate is two dimensional. In very large pores, for species that adsorb close to the pore wall, quantum confinement will occur radially but not angularly. In this case of one dimensional confinement, S_0 is given by

$$S_0=\sqrt{\frac{m_j}{m_i}}\exp\left[-\frac{E_i-E_j}{kT}\right], \tag{7}$$

where E_i is the ground-state energy due to quantization in the direction normal to the pore wall. This expression is also appropriate for adsorption on planar substrates.[3]

Two extensions of the results above are worth mentioning. First, the simple theory can be improved by relaxing the assumption that at low temperatures only ground states are populated. If E^l is the lth energy level for the quantized transverse motion, the chemical potential of the adsorbed component is given by

$$\mu_i^{\mathrm{ads}}=-kT\ln\left(\sum_l e^{-E_i^l/kT}\right)+kT\ln\left(\frac{\rho_i\lambda_i}{q_i}\right), \tag{8}$$

which reduces to Eq. (1) when only the ground state is populated. Considering the population of excited states, Eq. (8) is combined with Eq. (2) to give the selectivity S_0 as,

$$S_0=\frac{m_j}{m_i}\left[\frac{\sum_l \exp(-E_i^l/kT)}{\sum_l \exp(-E_j^l/kT)}\right]. \tag{9}$$

Second, additional contributions to the selectivity arise when the rovibrational states of adsorbed molecular species are affected by confinement.[3] In the calculations below dealing with SWNTs we have only considered translational degrees of freedom. It is useful to note in this context that recent experiments examining H_2 adsorption on bundles of SWNTs at cryogenic temperatures have found no significant barriers to quantum rotation in these systems.[35]

III. COMPUTING S_0 FROM PATH INTEGRAL SIMULATIONS

The theory presented above gives exact results for the selectivity of quantum sieving in noncorrugated micropores in the limit of low pressure, provided the energy levels of the adsorbed species can be determined. Since it is difficult to extend this theory to nondilute pore loadings or to pores with complex PESs, it is useful to consider numerical methods that can be applied to these systems. In this section we show how path integral Monte Carlo (PIMC) methods can be used to compute S_0. PIMC methods are not restricted to the dilute adsorption limit.[34]

The formalism of PI technique establishes an isomorphism between quantum statistical mechanics and the properties of classical ring polymers.[36] From this isomorphism, the canonical partition function for a system of N quantum particles can be approximated as

$$Q=\frac{1}{N!}\left(\frac{P}{\lambda^2}\right)^{3/2NP}\times V^N\int \ldots \int \exp[-\beta(U^{\mathrm{ext}}+U^{\mathrm{int}})]d\vec{s}_1\ldots d\vec{s}_N, \tag{10}$$

where P is the number of beads on a polymer-ring isomorph to a quantum particle with mass m, λ is the thermal de Broglie wavelength, $d\vec{s}=L^{-1}d\vec{r}\,d\omega\,d\Gamma$, a set of scaled coordinates with L the simulation-box length, $\vec{r}$ the center-of-mass vector of the ring polymer, ω representing the orientation Euler angles, and Γ, the internal conformation of the ring polymer. The intermolecular (external) potential is given by

$$U^{\mathrm{ext}}=\frac{1}{P}\sum_{\alpha=1}^{P}\sum_{i<j}^{N}\phi(r_{ij}^{\alpha})+\frac{1}{P}\sum_{\alpha=1}^{P}\sum_{i=1}^{N}\phi^{\mathrm{wall}}(r_i^{\alpha},\theta), \tag{11}$$

where $\phi(r_{ij}^{\alpha})$ is the adsorbate-adsorbate pair potential between bead α on molecule i and bead α on molecule j, r_{ij}^{α} is the scalar distance between the beads. $\phi^{\mathrm{wall}}(r_i^{\alpha},\theta)$ is the pore-adsorbate interaction potential. The intramolecular potential is

$$U^{\mathrm{int}}=\frac{mP}{2\beta^2\hbar^2}\sum_{\alpha=1}^{P}\sum_{i=1}^{N}|\vec{r}_i^{\alpha}-\vec{r}_i^{\alpha+1}|^2, \tag{12}$$

where $\vec{r}_i^{\alpha}$ is the position of bead α on ring i. When $\alpha=P$, $\alpha+1=1$ as required for a ring polymer.

For a mixture composed of N_1 particles of component 1 and N_2 particles of component 2, the partition function is

$$Q_{N_1,N_2}=\frac{1}{N_1!N_2!}\left(\frac{P}{\lambda_1^2}\right)^{3/2N_1P}\left(\frac{P}{\lambda_2^2}\right)^{3/2N_2P}V^{N_1+N_2}\times\int\exp[-\beta(U^{\text{ext}}+U^{\text{int}})]d\vec{s}_{N_1+N_2}. \tag{13}$$

Additionally,

$$\mu_1=-kT\ln\left(\frac{Q_{N_1+1,N_2}}{Q_{N_1,N_2}}\right)$$

and a similar expression for μ_2. The respective chemical potentials can be written now as

$$\mu_i=kT\ln\left\{(N_i+1)\left(\frac{\lambda_i^2}{P}\right)^{3/2P}\times\frac{\int\exp[-\beta(U^{\text{ext}}+U^{\text{int}})]d\vec{s}_{N_1+N_2}}{\int\exp[-\beta(U^{\text{ext}}+U^{\text{int}})]d\vec{s}_{N_1+N_2+1_i}}\right\}, \tag{14}$$

which applies for either component and in both the adsorbed as well as the bulk phase. In the bulk phase, which is assumed to be an ideal gas, U^{ext} is equal to zero. In the adsorbed phase, we assume the absence of adsorbate-adsorbate interactions due to low coverage. So, $U^{\text{ext}}=\phi^{\text{wall}}$. Since $\mu_{i,\text{ads}}=\mu_{i,\text{bulk}}$ for each component, the selectivity, S_0, can now be rewritten as

$$\begin{aligned}S_0&=\frac{x_1}{y_1}\frac{y_2}{x_2}=\frac{(N_1)_{\text{ads}}}{(N_1)_{\text{bulk}}}\frac{(N_2)_{\text{bulk}}}{(N_2)_{\text{ads}}},\\&=\frac{\int d\Gamma_1\int d\omega_1\int_0^R dr\int_0^{2\pi}r\,d\theta\exp[-U_1/kT]\Big/\int d\Gamma_1\exp[-U_1^{\text{int}}/kT]}{\int d\Gamma_2\int d\omega_2\int_0^R dr\int_0^{2\pi}r\,d\theta\exp[-U_2/kT]\Big/\int d\Gamma_2\exp[-U_2^{\text{int}}/kT]},\end{aligned} \tag{15}$$

where U_i is the sum of U^{int} and ϕ^{wall}. In the last step we have decomposed $d\vec{r}=r\,dr\,d\theta\,dz$, with dz canceling from the numerator and the denominator of each component, respectively.

One approach to evaluating S_0 is to directly determine the numerator and the denominator of Eq. (15) numerically. We have done this for a variety of pores by using quadrature integrals over r and θ and using Monte Carlo sampling of the ring configurations, Γ and ω, at each quadrature point. Although this method is formally valid, we have found it to be very inefficient, especially for systems where $S_0\gg 1$ (or equivalently, $S_0\ll 1$).

An alternative approach to evaluating S_0 is to rewrite Eq. (15) as

$$S_0=\frac{\int d\Gamma\int d\omega\int_0^{2\pi}r\,d\theta\int_0^R dr\exp[-U_2/kT]\exp[-\Delta U_{12}/kT]}{\int d\Gamma\int d\omega\int_0^{2\pi}r\,d\theta\int_0^R dr\exp[-U_2/kT]}=\langle\exp[-\Delta U_{12}/kT]\rangle_2. \tag{16}$$

Here, $C_{21}=\int d\Gamma_2\exp[-U_2^{\text{int}}/kT]/\int d\Gamma_1\exp[-U_1^{\text{int}}/kT]=(m_2/m_1)^{3(1-P)/2}$ is a constant derived from the ideal gas ring conformation distribution,[45] $\Delta U_{12}=U_1-U_2$, and $\langle\ldots\rangle_2$ represents an ensemble average over the phase space of component 2. This expression resembles the calculation of free-energy differences between two species or state points.[37] In the case of isotopic species, ΔU_{12} arises solely from the mass dependence of the intramolecular potential of the PI ring polymers [see Eq. (12)]. To evaluate Eq. (16) numerically, one would simulate a set of particles of component 2 interacting with the adsorbent and the intramolecular potential. Randomly transforming these particles into component 1 and evaluating the change in the intramolecular potential energy would then give ΔU_{12} for determining S_0. Instead of transforming a particle of component 2 to component 1 abruptly, a gradual transformation can be performed, which is analogous to the method of evaluating residual chemical potentials using ''Kirkwood ensemble integration.'' This

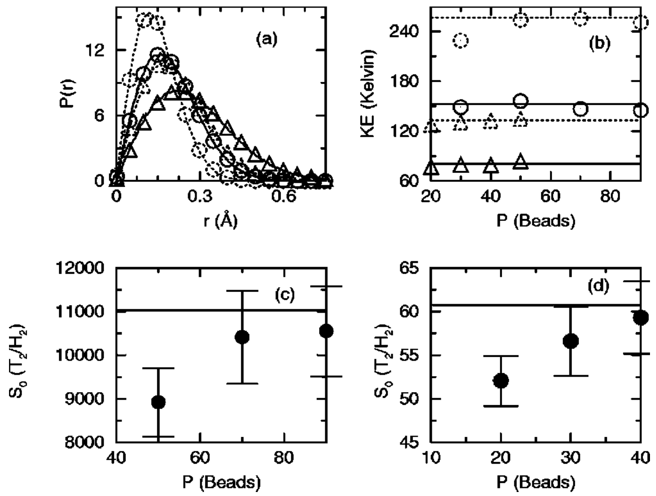

FIG. 1. Results for a 2-D harmonic potential. (a) Probability distribution (b) Kinetic energy. Circles are for the high-selectivity harmonic potential ($K = 10\,000$ K/Å ^{2}), and triangles for the low-selectivity potential ($K = 2500$ K/Å ^{2}). Solid and dotted symbols represent H_2 and T_2, respectively. Symbols are from PIMC simulations and lines are from simple theory. S_0 values from simple theory (solid lines) and Kirkwood integration (circles) for (c) the high selectivity potential and (d) the low selectivity potential.

new method has been found to be very efficient and accurate for calculating free energy changes.[38] Employing this method, the mass of component 2 is changed linearly from m_2 to m_1 in intervals and the change in energy is calculated as

$$\Delta U_{12} = \int_{m_2}^{m_1} \left(\frac{dU^{\text{int}}}{dm} \right) dm.$$

We describe the details of implementation of this method to calculate S_0 in the following section.

IV. RESULTS AND DISCUSSION

A. Harmonic potential

In order to test the convergence of our PIMC method, we have applied it to the simple case of a pore whose pore–adsorbate interactions are given by a two-dimensional (2D) harmonic oscillator, $\phi = \frac{1}{2} K r^2$. Two cases are considered, one with high selectivity ($K = 10\,000$ K/Å ^{2}) and another with low selectivity ($K = 2500$ K/Å ^{2}). We consider here the adsorption of particles with mass 2 amu and 6 amu, referred to below as H_2 and T_2, in this potential. For this simple potential, S_0 can be calculated exactly using Eq. (9) and the energy levels of a quantized harmonic oscillator. It is similarly straightforward to calculate the exact kinetic energies and adsorbate probability densities in the pore. Calculations were done for adsorption at 20 K and are shown in Fig. 1. At 20 K, the predominant occupancy was in the ground state. It is assumed that only two dimensions are quantized, and so there is still a contribution of $kT/2$ towards the kinetic energy from classical motion in the axial direction.

To compare these results for the H_2/T_2 system from the simple theory, we calculated the same properties, S_0, kinetic energies, and probability densities using path integrals. Kinetic energies in path integral simulations are based on the Barker energy estimator.[39] The simulation box consisted of 50 particles of T_2 at 20 K, which interact only with the pore. We used about 40–90 beads per particle, with larger number of beads being employed for highly selective systems. In each step, 25 particles were randomly chosen and transformed in gradual intervals from T_2 to H_2. After each interval involving a step change in mass, all the particles are moved in a hybrid MC manner at constant temperature. It is not necessary to equilibriate the system in these hybrid MC moves. The change in energy due to intramolecular potential is collected in each move for each interval. S_0 from each of these 25 particles is averaged for one step to get a mean S_0. Such steps were repeated for 100 times to get a final average of S_0 over 100 steps. At the end of each step, the transformed particles revert to their original states and the whole system is propagated by a single hybrid Monte Carlo step before the next step is performed. In this manner we sample the conformation space of path integrals extensively.

The comparisons for the three properties are illustrated in Fig. 1. The agreement between path integral calculations and the rigorous analytical calculations of quantum sieving is very good. However, it can be seen that for the high-selectivity case, one has to employ a large number of beads for accurate results. The number of beads required to converge the results increases as the system becomes more highly confined because quantum effects become more important. An insufficient number of beads leads to a lower selectivity from PI simulations compared to the selectivity obtained from the analytical calculations. However, simulation of systems with large number of beads becomes very expensive and time consuming. Additionally, as the number of beads increases, the number of intervals over which a T_2 is transformed to H_2 has to be increased to get a good estimate of the change in energy. From our simulations we found that about 500–5000 transformation/integral intervals have to be employed in the Kirkwood ensemble integration for good convergence in the high-selectivity case.

B. Quantum Sieving in SWNTs

In the remainder of this paper, we examine the quantum sieving selectivities of small molecules adsorbed in single-walled carbon nanotubes. Specifically, we consider isotopes of molecular hydrogen, helium, and methane. In each case, the interaction potentials for the various nanotubes were generated by summing pair-wise interaction between carbon atoms of the nanotube and species being adsorbed. For carbon-H_2 interactions, we used the Crowell-Brown potential.[40] This interaction potential has been used to model adsorption of hydrogen on graphite, and in carbon slit pores and nanotubes.[16,41] This potential accurately reproduces the adsorption isotherms for H_2 on graphite.[41] The interaction between carbon and methane molecules was modeled by a Lennard–Jones potential.[42] An anisotropic pair potential was used for interactions between He and C atoms.[43] Examination of the axial and angular corrugation of the PESs defined by our models indicates that these corrugations are negli-

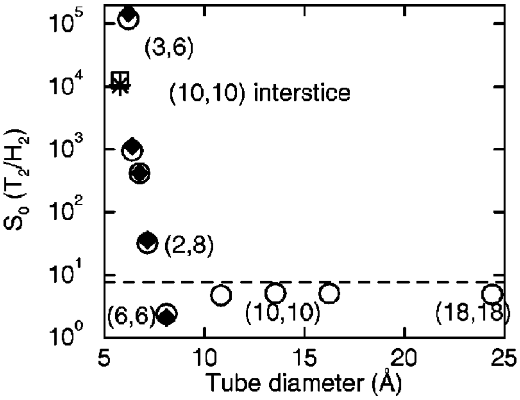

FIG. 2. S_0 at 20 K for T_2-H_2 as a function of tube diameter. Results from Eq. (9) (diamonds) and path integral calculations (circles) are shown. A few specific tubes are labeled on the graph with their (n,m) indices. S_0 in the (10,10) interstice is shown as an open square (PIMC) and an asterisk (simple theory).

gible. For example, the PES for H_2 in a (3,6) nanotube shows axial variations of only 0.01 K at the tube center and <1 K at $r=0.1$ Å. Accordingly, we defined smoothed potentials by performing axial and angular averaging for each tube. All results below for adsorption in SWNTs are based on these smoothed potentials.

For each smoothed potential $\phi(r)$ that exhibits a single minimum at $r=0$, we have computed S_0 using Eq. (9). The quantized energy levels of each adsorbed species were evaluated by expanding the species' wave function with a 2D harmonic oscillator basis set and computing the eigenvalues of the resulting Hamiltonian matrix.[44] We have included 30 energy levels in Eq. (9) to determine the zero-pressure selectivities. This number of states was found sufficient to give a converged value of S_0. Since Eq. (9) is inappropriate when $\phi(r)$ exhibits multiple minima, as is the case for wide pores, we have also computed S_0 using the PIMC methods described in Sec. III.

We first discuss quantum sieving of T_2 and H_2 in SWNTs. The mass ratio of T_2 to H_2 is the largest of all the isotope pairs we have considered, so it is not surprising that this system shows the strongest selectivities. S_0 for T_2-H_2 adsorption at 20 K is shown in Fig. 2 for SWNTs with a range of pore sizes. We have reported similar calculations,[2] but subsequently discovered a small error in the potential used in our earlier study. Figure 2 replaces Fig. 1 of Ref. 2. Our qualitative conclusions remain unchanged, although the corrected potential gives a higher selectivity in some SWNTs. The agreement between our PIMC results and Eq. (9) is excellent except for tubes with very large selectivities, where it is difficult to completely converge the PIMC sampling (see Sec. IV A).

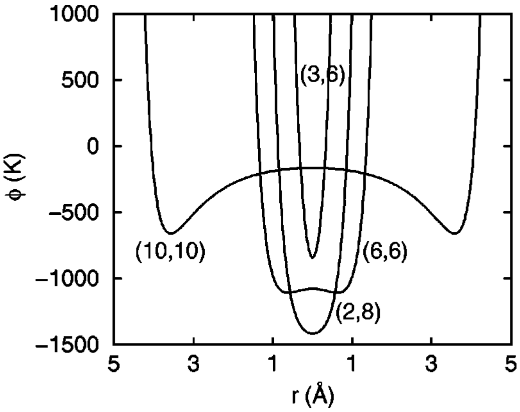

FIG. 3. Interaction potential inside carbon nanotubes between hydrogen isotopes and the nanotubes.

The most dramatic feature of Fig. 2 is the extremely large selectivities observed for small nanotubes. As the tube diameter is reduced below about 7 Å the adsorbed molecules are highly confined and therefore possess substantial zero-point energies. For tubes with diameters greater than 7 Å, molecules preferentially adsorb near the pore walls rather than in the pore center, leading to the type of 1D quantum confinement discussed in Eq. (7). For very large pores, the selectivity for T_2 over H_2 approaches that of planar graphite, as shown in Fig. 2 by the dashed line. It is interesting to note that the lowest selectivity occurs at the transition between 2D and 1D confinement, that is, in the (6,6) tube. In this tube, the adsorbate wave functions are more delocalized than in any other tube. The reason is, as shown in Fig. 3, the interaction potential inside the (6,6) nanotube is flatter and broader at the well compared to either narrower or wider tubes, which makes it an unlikely candidate for confinement of small molecules.

One unfortunate feature of Fig. 2 is that SWNTs with diameters less than 7 Å appear to be difficult to synthesize. Although the synthesis of 5-Å nanotubes has recently been reported,[14,15] most current syntheses yield much larger tubes. As we have previously noted,[2] high quantum sieving selectivities can also be achieved by allowing adsorption in the interstitial regions formed by ordered bundles of SWNTs. Nanotube bundles have been observed in numerous experiments.[10,27] One example of T_2-H_2 quantum sieving in the interstices of a nanotube bundle is shown in Fig. 2. We arranged (10,10) nanotubes in a 2-D triangular lattice with a gap between contact points equal to 3.2 Å, the van der Waals gap as observed in experiments.[10] Such an arrangement leaves an interstitial channel of 2.6 Å in diameter centered 9.676 Å from the center of each nanotube. The total interaction in the interstice is the sum of interactions due to three tubes, and the interaction potential has a threefold radial symmetry. It can be seen from Fig. 2 that the selectivity in this interstice is comparable to the highest selectivities observed inside the smallest SWNTs.

The predictions for the (10,10) interstices are based on a potential outside the nanotube that is averaged axially and angularly. We have calculated the corrugations in the PES of a fully atomistic model along the axis of the interstice at the interstice center. The corrugations in the PES depend on the orientations and relative axial alignment of the nanotubes. Calculations for various different orientations and alignments of the three nanotubes making up the interstice were performed. In all cases the van der Waals gap was held fixed at 3.2 Å. The maximum interstitial corrugation occurs when lines from each of the nanotube centers to the interstice cen-

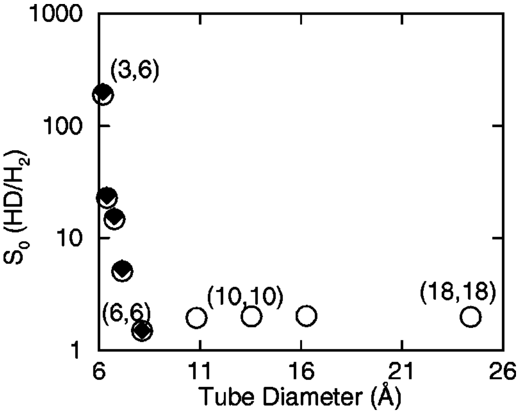

FIG. 4. S_0 at 20 K for HD-H_2 as a function of tube diameter. Results from Eq. (9) (diamonds) and path integral calculations (circles) are shown.

ter pass through the center of a graphitic hexagon and all three of these lines lie in the same plane. The corrugation in this case is about 306 K. However, the (10,10) nanotube has a D_{10h} (tenfold) symmetry, therefore, if one interstice has maximal corrugation none of its three neighboring interstices can have maximal corrugation. The probability of achieving the maximum corrugation is quite small. Furthermore, the minimum corrugation we observed for a (10,10) interstice is about 2 K. A random sampling of 10 000 orientations and axial alignments gave an average corrugation of about 100 K. In addition, real nanotube bundles are composed of nanotubes of various diameters and helicities, both of which would decrease the probability of observing maximal corrugations in the interstitial channels. The maximal corrugation of 300 K would certainly lead to axial confinement. The effect of such confinement would be to further enhance the selectivity; this would not change the qualitative picture of quantum sieving. The enhancement in selectivity due to axial confinement would be small because the second gradients of axial corrugations are small compared to the radial second gradients. Hence, the averaged potential is a good approximation to the atom explicit potential, but may slightly underestimate the selectivity due to neglect of axial confinement.

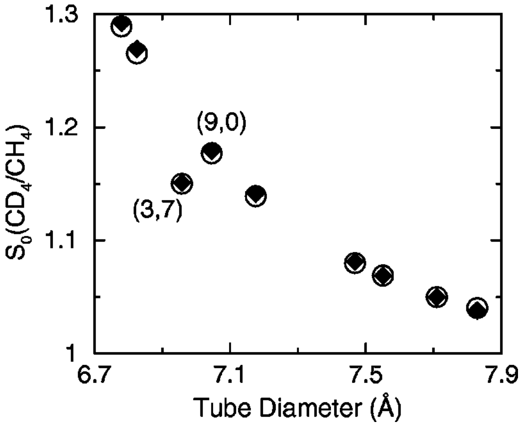

FIG. 5. S_0 at 90 K for CD_4-CH_4 as a function of tube diameter. Symbols are the same as in Fig. 4.

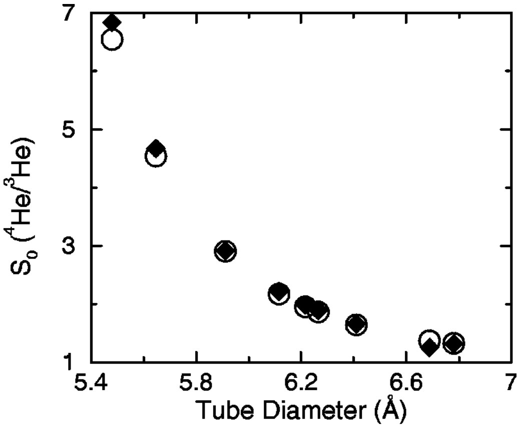

FIG. 6. S_0 at 20 K for ^{4}He-^{3}He as a function of tube diameter. Symbols are the same as in Fig. 4.

Similar to the T_2-H_2 mixture, the selectivity of HD over H_2 decreases rapidly with tube size, as shown in Fig. 4. The smaller mass ratio in the HD-H_2 system gives rise to lower selectivities compared to T_2-H_2, although still very high compared to selective adsorption on planar surfaces. The selectivities for the CH_4-CD_4, and ^{3}He-^{4}He systems in different nanotubes are shown in Figs. 5 and 6. Of the species we have examined, He has the smallest size, so to observe quantum confinement one has to explore extremely narrow tubes. For CH_4-CD_4, which is shown at 90 K, the selectivities are close to unity due to small mass ratio and the increased temperature relative to the results in Figs. 2, 4, and 6. The effect of tube diameter as well as the helicity of the graphite structure forming the nanotube can be seen in the CH_4-CD_4 system. Even though the (3,7) nanotube is smaller in diameter than the (9,0) nanotube, we see a lower selectivity for CD_4 in the smaller tube. This can be explained by the observation that in the narrower (3,7) nanotube, which is chiral, an adsorbed molecule is never directly on top of more than one carbon atom at a time. In contrast, the (9,0) nanotube is achiral (zigzag) and an absorbed molecule may be directly on top of 9 or 18 carbon atoms, depending on its axial loca-

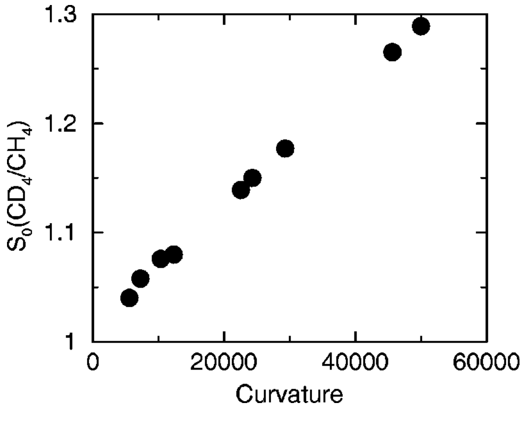

FIG. 7. S_0 at 90 K for CD_4-CH_4 as a function of curvature of the potential well. The second derivative of the potential at the minimum is taken as a measure of the curvature and shown on the abscissa in units of K/Å ^{2}.

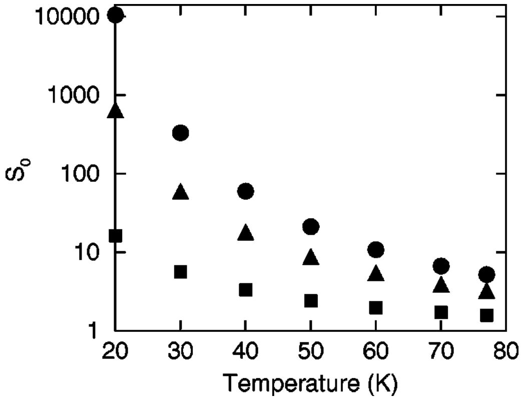

FIG. 8. S_0 in the (10,10) interstices as a function of temperature for T_2-H_2 (circles), HT-H_2 (triangles), and T_2-HT (squares).

tion in the nanotube. Hence, the (9,0) nanotube has a steeper (stiffer) potential than the (3,7) nanotube, even after axial and angular averaging of the potential has been carried out. In the selected range of tube diameters, this was the sole case where anomalous behavior due to helicity is observed. Hence we see that the tube diameter alone does not carry all the information about the interaction potential. The steepness of the potential is an important factor that in some sense accounts for chirality. An approximate way to include the steepness of the potential is by computing the second derivative of the potential at the potential minimum. We have plotted the selectivity as a function of the second derivative at the potential minimum in Fig. 7. The quantum sieving effect increases monotonically with curvature of the potential, unlike in Fig. 5 where the change in selectivity is not monotonic with tube diameter.

Quantum sieving effects decrease rapidly as the temperature increases. Using Eq. (9) we calculated S_0 for three different hydrogen isotope mixtures in the interstices of (10,10) nanotubes at different temperatures. The contribution from excited states becomes more important; and we have used 30 energy states, ensuring convergence with respect to energy states. The selectivity drops dramatically for H_2-T_2 mixture upon increasing the temperature, as shown in Fig. 8. The selectivity for T_2 over H_2 at 77 K is about 5.2, a mere 0.05% of the corresponding value at 20 K. As can be seen from Eq. (9), this strong temperature dependence of quantum sieving selectivity is a general property of adsorption of isotopic mixtures, not just a phenomenon that applies to carbon nanotubes. For example, the current observations suggest that the selectivity for D_2 over H_2 adsorbed in NaA zeolite that has been observed experimentally[7] at 77–120 K would be much more dramatic at lower temperatures.

V. CONCLUSION

We have presented a simple theory explaining the phenomenon of quantum sieving in narrow tubes and on 2D surfaces. This simple theory allows calculation of zero-pressure selectivity for mixtures, and the technique of quantum sieving is especially suited for separation of isotope mixtures. Using the rigorous analytical calculations of quantum sieving, carbon nanotubes of various sizes and helicities have been assayed for their ability to separate light-isotope mixtures of H_2-T_2, H_2-HD, ^{3}He-^{4}He, and CH_4-CD_4. The interactions between nanotubes and adsorbate particles have been modeled by realistic potentials. For each system considered, the nanotubes suitable for separation fall in a small range of tube diameters about the size of the particles in the system. Exceptionally high selectivities are predicted for systems like H_2-T_2 in narrow pores of (3,6) nanotubes and the interstitial regions of (10,10) nanotube bundles. Heavier systems like CH_4-CD_4 exhibit little quantum sieving effect in the nanotubes. The predictions from simple theory are in good agreement with detailed path integral calculations of S_0 for the systems considered here.

In this paper we have only discussed adsorption in the limit of low pressure/coverage, where adsorbate-adsorbate interactions can be neglected. To complement this work, we have used PIMC simulations to examine multicomponent adsorption of hydrogen isotopes in carbon nanotubes over a broad range of bulk pressures. These simulations show that the quantum sieving selectivities observed in the low-pressure limit are an excellent indicator of the equilibrium selectivity under more general conditions. The details of these PIMC simulations will be reported in a subsequent paper.[34]

ACKNOWLEDGMENTS

J.K.J. acknowledges support from the Army Research Office and the National Science Foundation through CAREER Grant No. CTS-9702239. Simulations were performed at the University of Pittsburgh's Center for Molecular and Material Simulations.

---

*Author whom correspondence should be addressed. Email address: karlj@pitt.edu

[1] J. J. M. Beenakker, V. D. Borman, and S. Yu. Krylov, Chem. Phys. Lett. **232**, 379 (1995).

[2] Q. Wang, S. R. Challa, D. S. Sholl, and J. K. Johnson, Phys. Rev. Lett. **82**, 956 (1999).

[3] D. White and E. N. Lassettre, J. Chem. Phys. **32**, 72 (1960).

[4] A. Katorski and D. White, J. Chem. Phys. **40**, 3183 (1964).

[5] J. King, Jr. and S. W. Benson, J. Chem. Phys. **44**, 1007 (1966).

[6] J. L. Maienschein, R. S. Hudson, R. T. Tsugawa, E. M. Fearon, P. S. Souers, and G. W. Collins, J. Vac. Sci. Technol. A **10**, 556 (1992).

[7] F. Stéphanie-Victoire, A-M. Goulay, and E. Cohen de Lara, Langmuir **14**, 7255 (1998).

[8] S. Iijima and T. Ichihashi, Nature (London) **363**, 603 (1993).

[9] D. S. Bethune, C. H. Kiang, M. S. de Vries, G. Gorman, R. Savoy, J. Vazquez, and R. Beyers, Nature (London) **363**, 605 (1993).

[10] A. Thess, R. Lee, P. Nikolaev, H. J. Dai, P. Petit, J. Robert, C. H. Xu, Y. H. Lee, S. G. Kim, A. G. Rinzler, D. T. Colbert, G. E. Scuseria, D. Tomanek, J. E. Fischer, and R. E. Smalley, Science **273**, 483 (1996).

[11] S. Amelinckx, X. B. Zhang, D. Bernaerts, X. F. Zhang, V. Ivanov, and J. B. Nagy, Science **273**, 483 (1994).
[12] S. C. Tang, P. J. F. Harris, and M. L. H. Green, Nature (London) **362**, 520 (1993).
[13] P. M. Ajayan, T. W. Ebbesen, T. Ichihashi, S. Iijima, K. Tanigaki, and H. Hiura, Nature (London) **362**, 522 (1993).
[14] L. M. Peng, Z. L. Zhang, Z. Q. Xue, Q. D. Wu, Z. N. Gu, and D. G. Pettifor, Phys. Rev. Lett. **85**, 3249 (2000).
[15] L. F. Sun, S. S. Xie, W. Liu, W. Y. Zhou, Z. Q. Liu, D. S. Tang, G. Wang, and L. X. Qian, Nature (London) **403**, 384 (2000).
[16] Q. Wang and J. K. Johnson, J. Chem. Phys. **110**, 577 (1999).
[17] Q. Wang and J. K. Johnson, J. Phys. Chem. B **103**, 4809 (1999).
[18] M. S. Dresselhaus, K. A. Williams, and P. C. Eklund, MRS Bull. **24**, 45 (1999).
[19] F. Darkrim and D. Levesque, J. Chem. Phys. **109**, 4981 (1998).
[20] G. Stan and M. W. Cole, Surf. Sci. **395**, 280 (1998).
[21] G. Stan and M. W. Cole, J. Low Temp. Phys. **110**, 539 (1998).
[22] A. C. Dillon, K. M. Jones, T. A. Bekkedahl, C. H. Kiang, D. S. Bethune, and M. J. Heben, Nature (London) **386**, 377 (1997).
[23] C. Liu, Y. Y. Fan, M. Liu, H. T. Cong, H. M. Cheng, H. M. Cong, and M. S. Dresselhaus, Science **286**, 1127 (1999).
[24] S. Inoue, N. Ichikuni, T. Suzuki, T. Uematsu, and K. Kaneko, J. Phys. Chem. B **102**, 4689 (1997).
[25] A. Kuznetsova, J. W. Yates, Jr., J. Liu, and R. E. Smalley, J. Chem. Phys. **112**, 9590 (2000).
[26] E. B. Mackie, R. A. Wolfson, L. M. Arnold, K. Lafdi, and A. D. Migone, Langmuir **13**, 7197 (1997).
[27] J. E. Fischer, H. Dai, A. Thess, R. Lee, N. M. Hanjani, D. L. Dehaas, and R. E. Smalley, Phys. Rev. B **55**, R4921 (1997).
[28] G. Stan, M. J. Bojan, S. Curtarolo, S. M. Gatica, and M. W. Cole, Phys. Rev. B **62**, 2173 (2000).
[29] G. Stan, V. H. Crespi, M. W. Cole, and M. Boninsegni, J. Low Temp. Phys. **113**, 447 (1998).
[30] W. Teizer, R. B. Hallock, E. Dujardin, and T. W. Ebbesen, Phys. Rev. Lett. **82**, 5305 (1999).
[31] S. Talapatra, A. Z. Zambano, S. E. Weber, and A. D. Migone, Phys. Rev. Lett. **85**, 138 (2000).
[32] H. Takaba, M. Katagiri, M. Kubo, R. Vetrivel, and A. Miyamoto, Microporous Mater. **3**, 449 (1995).
[33] K. G. Ayappa, Langmuir **14**, 880 (1998).
[34] S. R. Challa, J. K. Johnson, and D. S. Sholl (unpublished).
[35] C. M. Brown, T. Yildirim, D. A. Neumann, M. J. Heben, T. Gennett, A. C. Dillon, J. L. Alleman, and J. E. Fischer, Chem. Phys. Lett. **329**, 311 (2000).
[36] *Quantum Mechanics and Path Integrals*, edited by R. P. Feynman and A. R. Hibbs (McGraw-Hill, New York, 1965).
[37] *Computer Simulation of Liquids*, edited by M. P. Allen and D. J. Tildesley (Clarendon, Oxford, 1987).
[38] P. Diep, X. Zhao, S. Tulyani, and J. K. Johnson (unpublished).
[39] J. A. Barker, J. Chem. Phys. **70**, 2914 (1979).
[40] A. D. Crowell and J. S. Brown, Surf. Sci. **123**, 296 (1982).
[41] Q. Wang and J. K. Johnson, Mol. Phys. **95**, 299 (1998).
[42] H-Y. Kim and W. A. Steele, Phys. Rev. B **45**, 6226 (1992).
[43] M. W. Cole and J. R. Klein, Surf. Sci. **124**, 547 (1983).
[44] S. Hammes-Schiffer and J. C. Tully, J. Chem. Phys. **101**, 4657 (1994).
[45] Q. Wang, J. K. Johnson, and J. Q. Broughton, J. Chem. Phys. **107**, 5108 (1997).